CEE 588 final project (Spring 2018)

Local versus nonlocal tracer transport in the total energy-mass flux boundary layer scheme

Juho Iipponen
Program in Atmospheric and Oceanic Sciences
Princeton University, Princeton, NJ, United States

ABSTRACT

Transport of a moisture-like passive tracer is compared in local and nonlocal boundary layer schemes, based on an algorithm capable of separating the eddy diffusion and mass flux components. The nonlocal parameterization, including the effects of the convective updrafts, shows persistent deviations from the local scheme throughout the period when the boundary layer is convectively unstable. The local scheme, lacking the ventilating effect of the updrafts, produces a moister surface layer and a much drier entrainment zone than the nonlocal scheme. The moisture difference in the surface layer disappears as the boundary layer becomes stable, but the upper level discrepancy does not. Considering moisture as a passive tracer is proposed to qualitatively explain the similar results obtained in previous studies.

1. Introduction

The planetary boundary layer (PBL) acts as a coupler between the Earth's surface and the free troposphere. Thus, accurate representation of boundary layer processes is vital for predicting the large-scale weather and climate in numerical models (e.g. Hu et al., 2013). However, the turbulent processes in the PBL occur at scales not explicitly resolved by today's weather and climate models, whereby their effects on the mean flow have to be parametrized.

Several boundary layer schemes with varying complexities have been developed (see e.g. Cohen et al. (2015) for a review). The simpler parameterizations assume that the turbulent eddies mix scalars down the large-scale gradient, and that the magnitude of the transport is only a function of the local environment. Such local eddy diffusion schemes work reasonably well when the eddies are small relative to PBL height, but frequently fail when the transports depend on the environmental variables far away from the point of observation (e.g. Wyngaard and Brost, 1984). The most significant source of the non-local effects in the PBL is convection, which overturns a gravitationally unstable column of air, causing light air to rise and dense air to descend. When the surface is hotter than the air right above it, convection forms rising plumes, which, through strong mixing, create a well-mixed layer where the profiles of mean variables are strongly homogenized.

As the mean gradients diminish, they become poor predictors of the actual transports, and the simple eddy diffusion assumptions fail. Thus, more accurate modeling of the PBL requires the parameterization of the nonlocal fluxes induced by the convective plumes. In a seminal work, Holtslag and Boville (1993) compare the effects of a local and nonlocal scheme in a general circulation model, concluding that the result of the nonlocal fluxes is to transport moisture away from the surface layer to

the upper levels of the boundary layer. Comparing the predictions of the two schemes with observations, they find the lower layers to be unrealistically moist, a result having strong impacts on the boundary layer clouds and radiation. Since then, multiple studies with the aim of comparing local and nonlocal schemes in a weather model have been carried out (e.g. Hong and Pan, 1996; Hu et al., 2010; Xie et al., 2012; Banks et al., 2016)., essentially confirming the Holtslag and Boville (1993) conclusions.

The purpose of this study is to compare the local and non-local schemes in an idealized setting, not by comparing many different parameterizations, but only through a simple modification of one nonlocal scheme. The algorithm used in the project, the total energy-mass flux scheme (TEMF; Angevine et al., 2010, hereafter A10), combines down-gradient eddy diffusion with upward mass fluxes, assuming both processes play a role in mixing a convective boundary layer. As Huang et al. (2013) show, the TEMF, developed specifically for the simulation of marine boundary layer clouds, is capable of producing temperature and moisture profiles, which closely resemble the outputs of large-eddy simulations.

One of the main advantages of the TEMF algorithm is that the mass fluxes can easily be switched off for a particular scalar. In this work, the outputs of the TEMF scheme are compared for a moisture-like passive tracer in cases where the convective mass flux of the tracer is turned on or off. The central research question is to find out, where are the moisture deficits and excesses observed, when the model is driven in a local versus nonlocal setting. By toggling the mass flux only for the passive tracer, the problem is simplified as compared to previous studies, which often analyze completely different schemes each producing different thermal and kinematic structures. Despite of this key difference, we expect the Holtslag and Boville (1993) to hold, having strong physical reasons to support them.

2. The algorithm and experimental setup

2.1. The TEMF

The TEMF has been implemented as described in A10. At the heart of the algorithm lies an assumption that all vertical fluxes consist of a down-gradient eddy diffusion and a mass flux component:

$$\overline{w'\psi'} = -K\frac{d\psi}{dz} + M(\psi_u - \psi) \quad (1),$$

where w is the vertical velocity, ψ is any model scalar (velocities u or v, total turbulent energy E, potential temperature θ or passive scalar q) in the environment, ψ_u is the value of the scalar in the updrafts, M is the upward mass flux and K is the eddy diffusion coefficient. The mass flux scheme is activated only, when the boundary layer is convective (upward heat flux at the surface), whereby in a stable PBL, only down-gradient eddy fluxes are assumed to occur. To parameterize the eddy diffusion, Mauritsen et al. (2007) and A10 switched away from the prognostic description of the turbulent kinetic energy in favor of total turbulent energy E:

$$\frac{DE}{Dt} = -\overline{w'u'}\partial_z\bar{u} - \overline{w'v'}\partial_z\bar{v} - \gamma - \partial_z\overline{w'E'} + B \quad (2),$$

where the first two terms on the right are the shear production, the third term is the dissipation $(\gamma = 0.07 \cdot E^{3/2}/l)$, fourth term is the flux convergence (based on (1)) and $B = 2\frac{g}{\theta}\overline{w'\theta'}$ is the buoyancy production. Noteworthily, since the total turbulent energy (TTE) is defined as the sum of turbulent kinetic (TKE) and potential (TPE) energies, the buoyancy production term disappears in stably stratified conditions, when there is direct conversion between the TKE and TPE. According to A10, this improves the description of the eddy diffusion coefficients in the stable upper parts of a convective ABL, where the TKE is strongly damped.

The ratio of TPE to TTE can be described as a function of the gradient Richardson number, enabling the parameterization of the heat and momentum eddy diffusion (K_h and K_m, respectively) using velocity scales obtainable from turbulent energies (A10 equations (A12) and (A13)). In a stable PBL (downward sensible heat flux at the surface), the mixing lengths l (used to multiply the velocity scales to obtain the diffusion coefficients) are limited by the distance from the surface, Coriolis effect and local static stability. In convective situations, however, the length scale is assumed to be constrained only by the distances from the ground and the thermal top (h_d). Thus, in an unstable PBL, the diffusion coefficients simply become

$$K_m = f(Ri)\, l_{conv}\sqrt{E_k}$$
$$K_h = K_m / Pr_0$$

where E_k is the TKE and $Pr_0 = 0.69$ is the turbulent Prandtl number of a neutrally stratified atmosphere. K_m is used to diffuse the velocity and TTE, while K_h is used for potential temperature and the passive scalar.

The first step in the computation of the non-local fluxes is to compute the vertical profile of the convective mass flux M:

$$\frac{\partial M}{\partial z} = M(\epsilon - \delta) \quad (3)$$

using initial condition $M(z_0)=0.03\,w_*$ (where $w_*=\left(\frac{g}{\theta}h_d\overline{w'\theta'}\right)^{1/3}$ is the convective velocity). Here, the lateral entrainment (ε) and detrainment (δ) rates are parameterized based on LES results and height of the thermal top, typically being on the order of 10^{-3} (see A10 equations (A3) and (A4)). Then, the properties of the updraft are given by

$$\frac{\partial \psi_u}{\partial z}=-\epsilon(\psi_u-\psi) \quad (4).$$

The prognostic scalars u, v, θ and q develop according to:

$$\frac{\partial \bar{u}}{\partial t}=-\bar{w}\frac{\partial \bar{u}}{\partial z}+f(\bar{v}-v_g)-\frac{\partial \overline{u'w'}}{\partial z} \quad (5.1)$$

$$\frac{\partial \bar{v}}{\partial t}=-\bar{w}\frac{\partial \bar{v}}{\partial z}-f(\bar{u}-u_g)-\frac{\partial \overline{v'w'}}{\partial z} \quad (5.2)$$

$$\frac{\partial \bar{\theta}}{\partial t}=-\bar{w}\frac{\partial \bar{\theta}}{\partial z}-\frac{\partial \overline{\theta'w'}}{\partial z}-Q_{rad} \quad (5.3)$$

$$\frac{\partial \bar{q}}{\partial t}=-\bar{w}\frac{\partial \bar{q}}{\partial z}-\frac{\partial \overline{q'w'}}{\partial z} \quad (5.4)$$

The solution is characterized by the subsidence velocity $\bar{w}$, geostrophic velocities u_g and v_g, and radiative cooling Q_{rad},. Their combined effect is to prevent the PBL from growing without a bound during the model spin-up period, and to remove the heat deposited in the boundary layer by convection and entrainment. Free tropospheric lapse-rate at the model top is chosen to be 3 K/km, and it is assumed that above the boundary layer, subsidence heating approximately balances radiative cooling. Therefore we set $\bar{w}=-5$ mm/s at the model top (decreasing linearly to zero at the surface) and $Q_{rad}=-1.3\,\mathrm{K/d}$ throughout the model column (excluding the boundary points). Geostrophic velocity is chosen to only have a zonal component of 10 m/s.

The lowest model level is set to be at the roughness height $z_0=0.2$ mm, corresponding to a sea surface with a long fetch (WebMET.com, 2018). Both wind components are assumed to vanish at this level, and the surface temperature is specified by a sinusoidal function:

$$\theta_s=-\sin(2\pi t/1d)\cdot 6\,K+292.15\,K \quad (6)$$

Thus, the surface is heated from midday to midnight, reaching a maximum temperature of +25 ºC at 6 pm, and a minimum temperature of +13 ºC at 6 am. The tracer concentration at the lowest level is set at the saturation specific humidity of the surface.

The model uses a staggered grid, with the eddy fluxes and TTE defined at half levels, and the mean values and updraft fluxes defined at full levels. Vertical resolution of 10 meters is used throughout the boundary layer, the model top being at 3 km. Fluxes at the first turbulent half level are

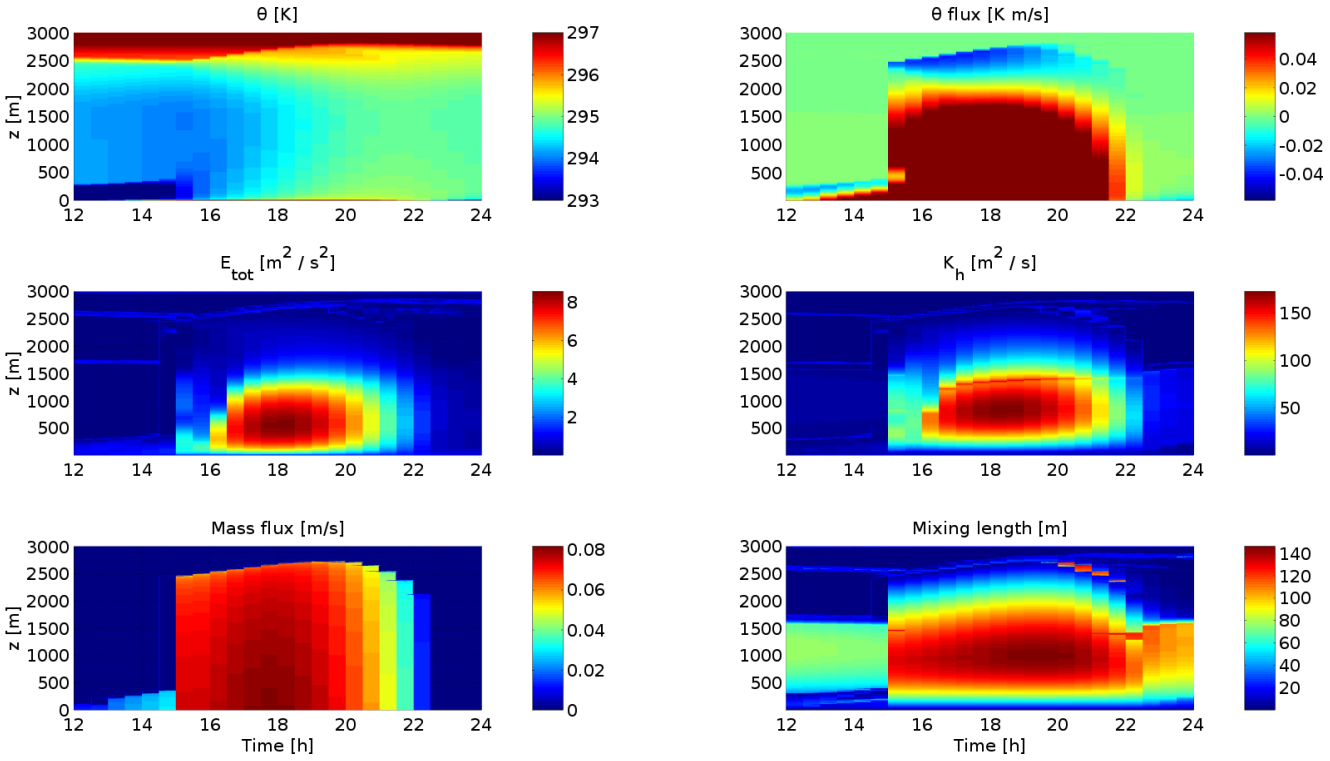

Figure 1. *Output of the TEMF scheme in convective daytime conditions. All of the shown variables are unaffected by the passive tracer, and are the same for both local and non-local runs.*

found by linearly interpolating between the first and second full levels, correcting for stability (see A10 equation (A23)). First-order finite differences are used to compute the gradients, and the model is integrated forward using the Euler method with a time step of 0.1 seconds.

Spin-up of three days is required for the PBL to reach a state in which the consecutive days look almost identical in terms of boundary layer height and thermal structure. The moisture-like tracer, however, increases slowly over time, because there is no removal process in the night-time residual layer. This slow tendency will not pose an issue, if we analyze only a single day; the results for the consecutive days are qualitatively very similar (not shown).

2.2. Experiments

To evaluate the changes in the profiles of tracer (q) with local and non-local mixing, we perform two experiments; one where the mass flux scheme is active in the tracer flux equation (1) (nonlocal scheme, hereafter subscript “NL”), and another where it is not (local scheme, hereafter subscript “L”). In both simulations, the three-day spin-up period includes the tracer mass flux, which is deactivated at the beginning of the fourth simulation day for the other experiment.

It should be stressed that the eddy diffusion coefficients in (1) are the same for both runs, since the mass fluxes are still active in driving the other prognostic variables (u, v, TTE, θ), whose time evolution is completely independent from that of the passive tracer.

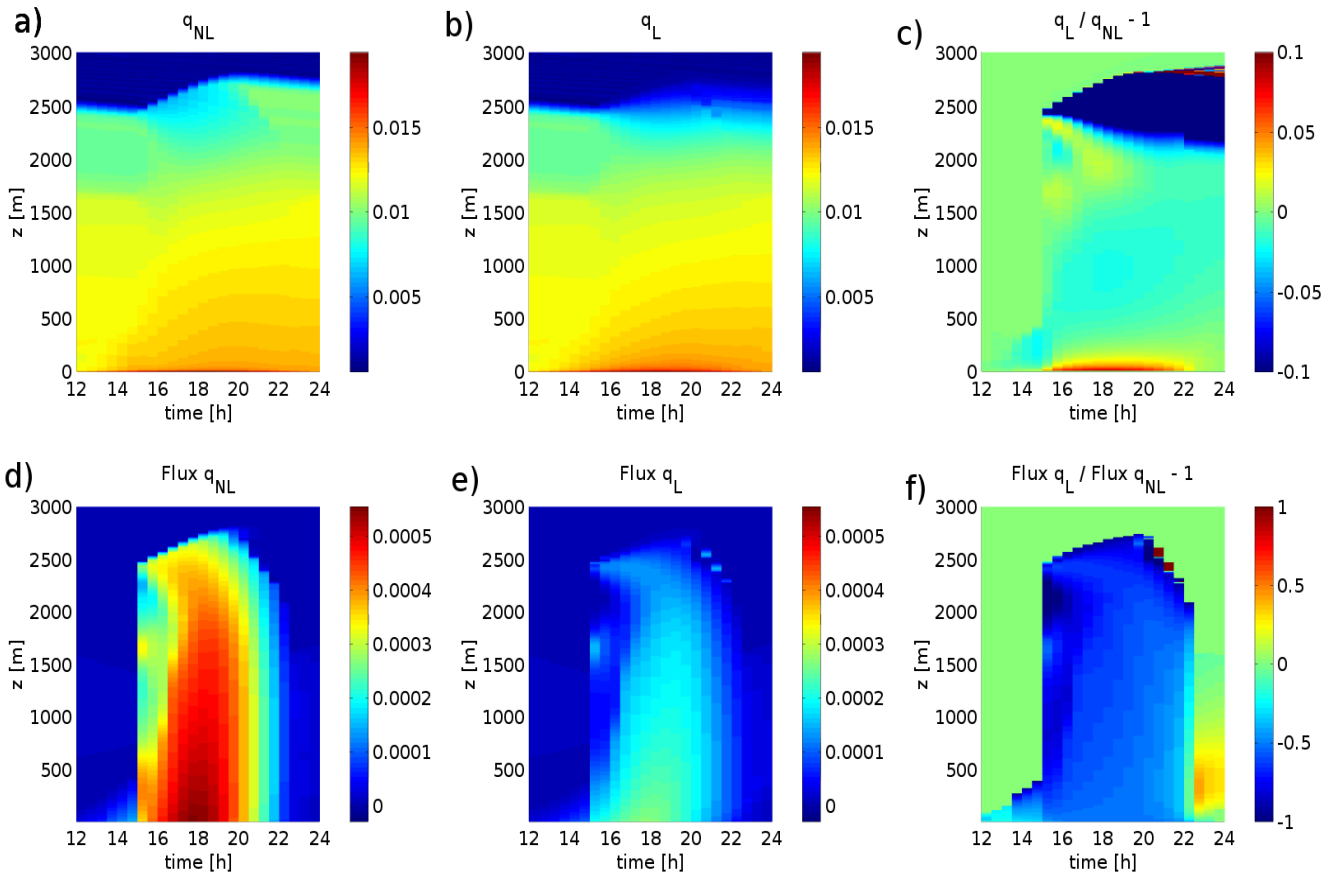

Figure 2. *Tracer concentrations for non-local (a) and local (b) transport and the associated vertical eddy fluxes (d) and (e). Panels (c) and (f) depict relative changes from local to non-local experiments.*

3. Results and Discussion

Figure 1 shows the time evolution of six parameters relevant to mixing in the TEMF. The analysis starts at noon, when the surface becomes warmer than the overlying air, changing the regime of the PBL from stable to convective. However, for the three hours following noon, the boundary layer remains shallow, as the thermals cannot penetrate through the stable layer created during the night. At the moment the convective plumes are able to reach the residual layer, the PBL (along with the heat and mass fluxes) experiences rapid growth. From Figure 1, the top of the entrainment zone (region of negative heat flux) steadily increases with time after this point (until 1900 hours), but the bottom of the zone (altitude of the zero-crossing of the heat flux) remains at a near-constant height. During this period, the potential temperature and stability of the entrainment zone increase due to mixing with the warm free-tropospheric air.

Based on Figure 1, the TTE and K_h change more slowly than the mass flux from about 1500 to 1630 hours, but they both reach a maximum value near the time of maximum surface heat flux (1800 hours). As the surface temperature and heat flux start to decrease, so does the convective mass flux,

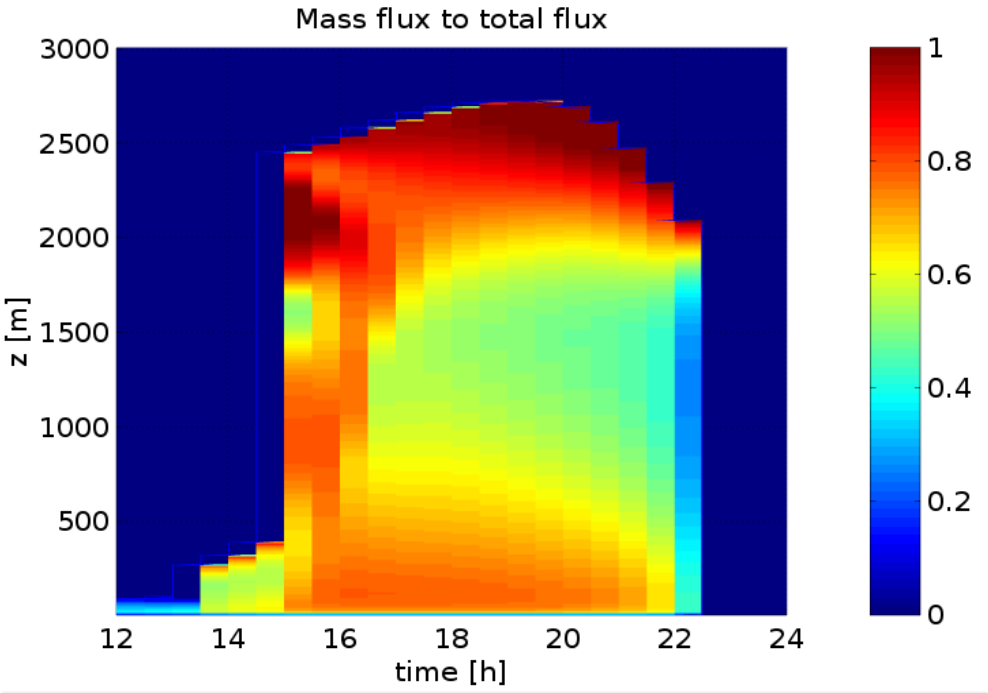

Figure 3*. Contribution of the mass flux to the total tracer flux in the nonlocal transport scheme.*

driving decreases in TET and K_h. After the surface layer has become stable (at around 2200 hours), elevated K_h values are observed in the residual layer.

Figure 2 shows the tracer concentrations and fluxes from the local and non-local experiments, together with their relative changes. Relatively small differences in concentration are observed in the first few hours after noon, when the thermals do not penetrate to the residual layer. However, the differences between the schemes grow stronger with the increased PBL height after 1500 hours. Largest deviations (Figure 2c) occur in the surface layer and in the entrainment zone, the former being more moist (up to 8 %) in the local scheme, while the latter being significantly drier (up to -80 %). The moist anomaly near the ground remains quite shallow, reaching a height of ~100 meters in the afternoon, with very little variation in amplitude at a given height. The upper level deviations grow in amplitude and in depth, following the growth of the entrainment zone. Nevertheless, after convection starts to diminish (at around 2000 hours), the deviation does not shrink with the entrainment zone, but large differences remain. This is in contrast with the surface layer anomaly, which quickly disappears after the lower layers become stable (at 2200 hours).

Differences between the two schemes are evident in the vertical fluxes. From Figures 2d-f it is clear that the fluxes are predominantly larger in the nonlocal run, by approximately a factor of two. Differences are larger right after the rapid growth of the boundary layer, but become slightly less pronounced in the late afternoon and evening. After the convection shuts down, there is considerable upward eddy flux in the residual layer of the local scheme, attributable to the stronger concentration gradient in the lower PBL.

To better understand the physical mechanism driving the discrepancies, Figure 3 depicts the ratio of the convective mass flux to the total (eddy and mass) flux in the case of the nonlocal scheme. Although the local eddy fluxes are not the same in the local and nonlocal runs, the differences between the two can be understood by only analyzing the nonlocal scheme. The figure explains much of the observed flux differences (Figures 2d-f), as the regions of large mass flux mostly coincide with the large changes in tracer flux between the two schemes. The mass flux becomes significant during and right after the period of rapid PBL growth, but at later times (after 1630 hours), a bimodal structure appears. The relative importance of the mass flux starts to decrease in the mixed layer, but in the entrainment zone and lower parts of the PBL, much of the flux is still carried by the rising thermals. Near the ground and in the entrainment zone, the eddy diffusion coefficients are small (due to lower turbulent energies and especially due to shorter mixing lengths, see also Figure 1), preventing strong down-gradient transport. Thus, the effect of the thermals is to carry the tracer away from the surface into the entrainment zone, drying the surface layer, and moistening the upper levels.

This result was expected, based on physical arguments and previous research. Quantitative comparisons, with, for example, the Holtslag and Boville (1993) study are difficult to make due to large differences in methodology and the amount of realism. In the real atmosphere, moisture is far from being a passive tracer, having indirect effects on other fields through processes like radiation, condensation and cloud formation. However, an idealized study such as this one serves as an important verification that it is the direct effects of the convective mass fluxes that explain much of the differences between the local and nonlocal schemes.

4. Summary and Conclusions

Local and nonlocal tracer transports are compared in the total energy-mass flux (TEMF) boundary layer scheme. Two idealized experiments are performed in a convective PBL, one where the mass flux is allowed to advect a moisture-like tracer, and another, where the effects of the mass flux have been switched off. Pronounced differences are observed between the two schemes, especially in the lower and upper parts of a convective boundary layer. Based on our analysis, we obtain the following main results and conclusions:

1. In the local scheme, the lower PBL remains moist throughout the convective day (as compared to the nonlocal experiment), but the difference between the two schemes quickly disappears as the stable nocturnal boundary layer forms.

2. The local scheme predicts a significantly drier entrainment zone, with the difference between the schemes growing as a function of time.

3. Thermals and the upward mass flux associated with them play a major role in transporting moisture in the vertical. They are the primary method of ventilating the surface layer, and fluxing tracers into the entrainment zone.

The results are qualitatively in line with previous studies (e.g. Holtslag and Boville, 1993), highlighting the sensitivity of a boundary layer simulation to the selection of the PBL scheme. As all of the differences presented herein are due to the direct effects of the mass flux, there is a reason to believe that much of the discrepancies between local and nonlocal moisture transport can be explained by considering moisture as a passive tracer, ignoring its impacts on other fields.

Acknowledgements

The full Fortran source code along with the data files used to produce the results is available at: https://github.com/juppiega/atmosphericModel

References

Banks, R. F., Tiana-Alsina, J., Baldasano, J. M., Rocadenbosch, F., Papayannis, A., Solomos, S., & Tzanis, C. G. (2016). Sensitivity of boundary-layer variables to PBL schemes in the WRF model based on surface meteorological observations, lidar, and radiosondes during the HygrA-CD campaign. *Atmospheric research*, *176*, 185-201.

Cohen, A. E., Cavallo, S. M., Coniglio, M. C., & Brooks, H. E. (2015). A review of planetary boundary layer parameterization schemes and their sensitivity in simulating southeastern US cold season severe weather environments. *Weather and forecasting*, *30*(3), 591-612.

Holtslag, A. A. M., & Boville, B. A. (1993). Local versus nonlocal boundary-layer diffusion in a global climate model. *Journal of Climate*, *6*(10), 1825-1842.

Hong, S. Y., & Pan, H. L. (1996). Nonlocal boundary layer vertical diffusion in a medium-range forecast model. *Monthly weather review*, *124*(10), 2322-2339.

Hu, X. M., Nielsen-Gammon, J. W., & Zhang, F. (2010). Evaluation of three planetary boundary layer schemes in the WRF model. *Journal of Applied Meteorology and Climatology*, *49*(9), 1831-1844.

Hu, X. M., Klein, P. M., & Xue, M. (2013). Evaluation of the updated YSU planetary boundary layer scheme within WRF for wind resource and air quality assessments. *Journal of Geophysical Research: Atmospheres*, *118*(18).

Huang, H. Y., Hall, A., & Teixeira, J. (2013). Evaluation of the WRF PBL parameterizations for marine boundary layer clouds: Cumulus and stratocumulus. *Monthly Weather Review*, *141*(7), 2265-2271.

Mauritsen, T., Svensson, G., Zilitinkevich, S. S., Esau, I., Enger, L., & Grisogono, B. (2007). A total turbulent energy closure model for neutrally and stably stratified atmospheric boundary layers. *Journal of the Atmospheric Sciences*, *64*(11), 4113-4126.

WebMET.com – the meteorological resource center, Meteorological Data Processing – Surface Roughness Length, Table 6-10, available online at: **http://www.webmet.com/met_monitoring/663.html**, fetched 05/13/2018.

Wyngaard, J. C., & Brost, R. A. (1984). Top-down and bottom-up diffusion of a scalar in the convective boundary layer. *Journal of the Atmospheric Sciences*, *41*(1), 102-112.

Xie, B., Fung, J. C., Chan, A., & Lau, A. (2012). Evaluation of nonlocal and local planetary boundary layer schemes in the WRF model. *Journal of Geophysical Research: Atmospheres*, *117*(D12).